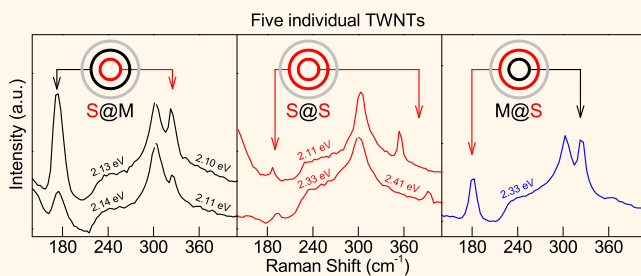


Characterization of Bundled and Individual Triple-Walled Carbon Nanotubes by Resonant Raman Spectroscopy

Thomas Ch. Hirschmann,^{†,§,*} Paulo T. Araujo,^{†,*} Hiroyuki Muramatsu,[‡] Xu Zhang,[†] Cornelius Nielisch,[§] Yoong Ahm Kim,[‡] and Mildred S. Dresselhaus^{†,§,*}

[†]Department of Electrical Engineering and Computer Science and [‡]Department of Physics, Massachusetts Institute of Technology, Cambridge, Massachusetts 02139-4307, United States, [§]Institute of Applied Physics, University of Hamburg, 20355 Hamburg, Germany, [†]Department of Materials Science and Technology, Nagaoka University of Technology, 1603-1 Kamitomioka, Nagaoka 940-2188, Japan, and [‡]Faculty of Engineering, Shinshu University, 4-17-1 Wakasato, Nagano 380-8553, Japan

ABSTRACT The optical characterization of bundled and individual triple-walled carbon nanotubes was studied for the first time in detail by using resonant Raman spectroscopy. In our approach, the outer tube of a triple-walled carbon nanotube system protects the two inner tubes (or equivalently the inner double-walled carbon nanotube) from external environment interactions making them a partially isolated system. Following the spectral changes and line-widths of the radial breathing modes and G-band by performing laser energy dependent Raman spectroscopy, it is possible to extract important information as regards to the electronic and vibrational properties, tube diameters, wall-to-wall distances, radial breathing mode, and G-band resonance evolutions as well as high-curvature intertube interactions in isolated double- and triple-walled carbon nanotube systems.



KEYWORDS: triple-walled carbon nanotubes · double-walled carbon nanotubes · resonant Raman · intertube interactions · wall-to-wall distances

A double-walled carbon nanotube (DWNT) consists of two concentric and weakly coupled (van-der-Waals interaction) single-walled carbon nanotubes (SWNTs). It is the simplest system in which to study the interaction between concentric layers in carbon nanotubes. The inner and outer nanotubes can be either semiconducting (S) or metallic (M), and each of the four possible flavors (S@S, M@M, S@M, and M@S) provides a multitude of information regarding their electrical, vibrational, and optical properties. Because the outer nanotube is in direct contact with the environment, additional interactions from the surroundings can affect the outer nanotube's properties and as a consequence the DWNT. To study the fundamental properties of an isolated DWNT and because of others interests, we produced an ensemble of a DWNT concentric to an external SWNT: a triple-walled carbon nanotube (TWNT).

TWNTs offer an ideal structure to study and understand how an interacting medium influences the general properties of both SWNT and DWNT structures as well as other hybrid systems and their mutual relationship. Unrolled, these TWNTs could be envisioned as a trilayer graphene ribbon. Note that, trilayer graphene is a material with outstanding properties and interesting for nanoelectronic applications.^{1–3} Because the inner and middle tubes are not in direct contact with the substrate and external environment, we assume that there is a negligible tube-substrate and external environment interaction for the two inner tubes. In this work we will show that for these inner tubes a flavor-dependent shielding phenomena might be taking place. However, we cannot assume the same situation for the outer tube, which is sitting on the substrate (individual case) or is in contact with other outer tubes (bundled case) and is subjected

*Address correspondence to
thirschm@physnet.uni-hamburg.de,
ptaraujo@mit.edu,
millie@mgm.mit.edu.

Received for review December 2, 2012
and accepted January 13, 2013.

Published online January 14, 2013
10.1021/nn3055708

© 2013 American Chemical Society

to other interactions with the external environment. Our results confirm some proposed properties for DWNTs which make them more interesting for numerous applications.⁴ A comparison of the TWNT results with the results for SWNTs and DWNTs, as observed in the literature, is addressed. Moreover, in this work we will focus on these inner DWNTs (inner@middle). We have experimentally characterized *via* resonant Raman spectroscopy (RRS) five individual, inner DWNTs which consist of three (S@M, S@S, and M@S) out of the four possible DWNT flavors.

Here by using laser energy (E_{laser}) dependent RRS, we explore the differences and similarities of bundled and individual TWNT species with their double and single walled counterparts. The radial breathing modes (RBMs, coherent breathing of the carbon atoms normal to the tube circumference, which is a special signature for carbon nanotubes), the D-band (disorder-induced), and the G-band (comprising the longitudinal optical (LO) and the tangential optical (TO) phonon modes) will be used as guides to our comparisons and understanding of the TWNTs and their differences and similarities with DWNT and SWNT systems.

The RBM is the most important spectroscopic signature of a carbon nanotube, whose frequency of vibration is known to be inversely proportional to the tube diameter (d_t).⁵ These first order Raman features provide a wealth of information on the nanotube electronic and vibrational structure, since, through their resonance patterns, one can assign the tube (n,m) indices based on detailed studies thoroughly provided on SWNTs.^{6–8} Our experimental results for RBM frequencies (ω_{RBM}) allow us to infer that the wall-to-wall (WtW) distance in the TWNT systems ranges from 0.323 to 0.337 nm between the two inner tubes of individual TWNTs. These results also confirm a theoretical study⁹ in which the coalescence process of fullerenes predicted to produce peapod-derived DWNTs is analyzed. The G-band Raman spectra will help us to confirm the electronic structure of the individual, inner DWNTs and to understand in depth how the environment surrounding the tubes is changing their properties. We observed E_{laser} -dependent changes of the G-band components, especially the G[–] occurrence for the semiconducting tubes (TO-related modes). The absence of significant D-bands underlines that the synthesized TWNTs are of high-quality and are a good choice for providing the fundamental information we seek in this study.

RESULTS AND DISCUSSION

After about one decade of experience with the production of peapod-derived DWNTs,¹⁰ this growth process is technically mature and we are now able to extend this knowledge to produce TWNTs by producing diameter-enlarged DWNTs as a hosting material for encapsulating fullerenes.¹¹ It is worth mentioning that theoretical and experimental studies^{9,12} demonstrate

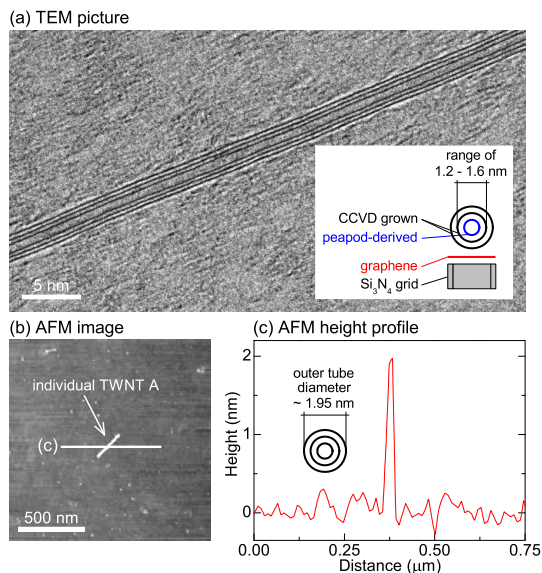


Figure 1. (a) TEM picture of an individual TWNT on top of a CCVD grown single layer of graphene which was placed on a Si₃N₄ grid. A schematic cross sectional view of the TWNT constituents and fabrication details are seen in the inset. (b) AFM picture of one individual TWNT and (c) the AFM height profile. In part b, the white solid line works as a guide to the eyes and it is properly scaled with the TWNT dimensions.

that the adjacent fullerenes in the hollow core of tubes are merged to form linear tubes *via* a thermal energy mechanism. In Figure 1a a transmission electron microscopy (TEM) picture of an individual TWNT is shown on top of a catalytic chemical vapor deposition (CCVD) grown monolayer of graphene prepared on a silicon nitride TEM grid. An atomic force microscopy (AFM) picture of one individual TWNT on the Si substrate can be seen in Figure 1b. The related AFM height profile can be seen in Figure 1c.

To measure the **bundled TWNTs** with our micro-Raman setup, we deposited the as-grown TWNT material on a microscope glass coverslip substrate. To avoid heating effects of the tubes, we used a laser power of about 1 mW to take the Raman spectra. By measuring the bundled TWNTs sample with an E_{laser} range from 1.55 to 2.54 eV, we extracted important information in the low frequency range from 160 to 410 cm^{–1} about the ω_{RBM} of each resonant (n,m) tube as well as its ($2n+m$) family. The Kataura plot¹³ is shown in Figure 2 on top of a two-dimensional color map, which represents the RBM intensity as a function of E_{laser} and ω_{RBM} for each laser excitation energy used here. The Kataura plot is based on the extended tight binding model,¹⁴ including many-body and curvature corrections, and such maps have been largely utilized to guide the (n,m) indices assignment of SWNTs^{15–17} and DWNTs.^{18–21} This theoretical plot shows the optical transition energies (E_{ii}) of each distinct (n,m) carbon nanotube as a function of its respective tube diameter, where $i = 1, 2, 3, \dots$ denotes the intersubband transitions between the i th valence and conduction

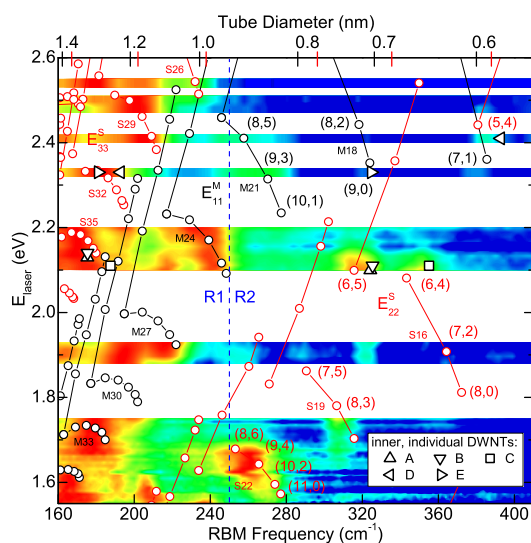


Figure 2. The calculated Kataura plot is shown on top of the experimental 2D map bringing the intensities of bundled TWNTs plotted as a function of the experimental E_{laser} vs ω_{RBM} . We listed some key (n,m) indices for some tubes and the points are plotted with their $(2n+m) = \text{constant}$ families indicated. The red and black thin-lines connect SWNTs belonging to the same semiconducting and metallic $(2n+m) = \text{constant}$ family. The red (blue) color scale of the Raman signal intensity corresponds to regions of maximum (minimum) RBM intensities that are observed experimentally. Each of the five symbols, labeled with capital letters (A–E), represent the inner and middle tubes of the five individual TWNTs that were studied in detail (see the bottom right corner). The upper scale represents the tube diameter according to eq 1 with region- and metallicity-dependent C_e values, as described in the main text.

bands for a given SWNT species. The RBM intensities of all spectra given by the 49 different E_{laser} lines that were used are normalized to the strongest peak, and plotted on a logarithmic scale. Because the Kataura plot is structured in order to show $(2n+m)$ family patterns, these family patterns can be used as anchors to help the comparison between experiment and theory (this procedure is explained in detail in ref 17). After applying the theory¹⁷ to the experiment, we find useful information about metallicity as well as the more likely flavors being observed through the color map.

In Figure 2 we see two distinct RBM scenarios: One region from 160 to 250 cm^{-1} (R1), in which the ω_{RBM} features overlap with each other and another region from 250 to 410 cm^{-1} (R2), in which the ω_{RBM} features are clearer so that information from the spectral features are easier to understand and extract. R2 corresponds to the inner peapod-derived tubes, and these tubes have diameters smaller than 0.95 nm. By using Lorentzian line shapes to fit the spectra of the bundled TWNTs taken with $E_{\text{laser}} = 2.10$ eV, a full width at half-maximum (fwhm) intensity at $\omega_{\text{RBM}} = 318.1$ cm^{-1} of the (6,5) tube is found to be 14 cm^{-1} , while a fwhm at $\omega_{\text{RBM}} = 350.5$ cm^{-1} for the tube (6,4) is observed to be 9 cm^{-1} . A broadening of one identified (n,m) tube can be explained by different metallicities of the

neighboring tube in combination with intertube interaction because of various WtW distances.^{18–24} Low temperature RRS measurements on DWNTs showed that this broadening can split into fine structured RBM clusters and one cluster consists of up to 14 clearly distinct components.^{21–24} We know from peapod-derived DWNTs that the RBMs of the inner tubes upshift (down-shift) because of increasing (decreasing) intertube interaction by smaller (larger) WtW distances.^{19–23} The RBM intensities in R1 mainly represent the middle tubes, and this diameter distribution is in accordance with the CCVD growth method used to grow diameter-enlarged DWNTs. More than that, these results reflect and confirm details of the peapod synthesis method, where depending on the host tube's diameter, the encapsulated inner tube is constrained to have just a few (n,m) configurations. In addition, the high frequency range from 1250 to 1650 cm^{-1} of bundled TWNTs shows a very weak distinctive D-band, which implies the high-quality of the TWNTs. The D-band shows a linear dependency of E_{laser} , respectively, $\omega_D = 1212.5 + 54.0 E_{\text{laser}}$.

We next discuss the relation between the measured ω_{RBM} as a function of d_t , which is important for finding the best Kataura's plot (seen in Figure 2) to be used in the (n,m) assignments for the isolated tubes. First, to get this ω_{RBM} vs d_t relation for the inner peapod-derived tubes (RBM intensities in R2 with $d_t < 0.95$ nm and $\omega_{\text{RBM}} > 250$ cm^{-1}), we correlated all clearly distinct RBMs from the bundled TWNTs together with published values of bundled peapod-derived DWNTs^{19,21} using the following relation,¹⁷

$$\omega_{\text{RBM}} = \frac{227}{d_t} \sqrt{(1 + C_e d_t^2)} \quad (1)$$

This relation comes from supergrown²⁵ SWNTs and in eq 1, $d_t = 0.142((3(n^2 + nm + m^2))^{1/2})/\pi$ is written in terms of the (n,m) indices and C_e is the only adjustable constant, which is related to environmental effects due to the nanotube interactions.¹⁷

We plotted in Figure 3 the experimental ω_{RBM} as a function of d_t and we noticed that metallic and semiconducting RBMs behave differently from each other so different C_e values were obtained for different tube metallicities. Fitting the data with eq 1 we obtain the C_e values $C_e^{S,R2} = 0.143 \text{ nm}^{-1}$ and $C_e^{M,R2} = 0.025 \text{ nm}^{-1}$ for semiconducting and metallic tubes, respectively. This indicates that semiconducting tubes are more affected by high-curvature intertube interactions than metallic tubes suggesting that a metallicity-dependent shielding phenomena might be taking place. Hence, the inner metallic tubes in DWNT and TWNT systems are more shielded by another outer concentric tube and can be seen to behave as more isolated tubes than inner semiconducting tubes. This property could be interesting for nanoscience applications with DWNTs and TWNTs. Regarding R1 in Figure 2, we fitted the RBM intensities for the middle CCVD grown tubes of the bundled TWNTs (with $d_t > 0.95$ nm and

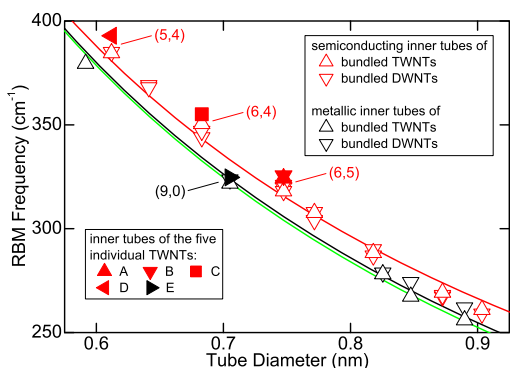


Figure 3. Experimental ω_{RBM} values for bundled peapod-derived tubes in DWNT and TWNT systems as a function of d_t . The red (black) line represents, according to eq 1, the fittings for semiconducting (metallic) inner tubes with $C_e^{8,R2} = 0.143 \text{ nm}^{-1}$ ($C_e^{9,R2} = 0.025 \text{ nm}^{-1}$). The green line depicts the relation $\omega_{\text{RBM}} = 227/d_t + 0.3 \text{ cm}^{-1}$ for supergrown²⁵ SWNTs (ref 16). We also included as filled symbols, the values of the inner tubes of the five individual TWNTs.

$\omega_{\text{RBM}} < 250 \text{ cm}^{-1}$) also with eq 1. Remember that the middle and outer tubes grow simultaneously *via* our CCVD growth method as mentioned earlier in the text. Semiconducting and metallic tubes follow the ω_{RBM} vs d_t relation with the environmental effect constants given by $C_e^{8,R1} = 0.097 \text{ nm}^{-1}$ and $C_e^{9,R1} = 0.065 \text{ nm}^{-1}$. The relation for middle metallic nanotubes is in good agreement with the widely utilized relation $\omega_{\text{RBM}} = 218.3/d_t + 15.9 \text{ cm}^{-1}$ for individual and bundled DWNTs.²⁶ Note that in comparison with the C_e values from the R2 inner tubes, an increase of the environmental effects of the metallic middle tubes is observed. This could likely be due to flavor-dependent interactions from the concentric inner and outer tubes. Semiconducting middle tubes show a smaller environmental effect dependence, which confirms the significant high-curvature intertube interactions of semiconducting inner tubes. Another important observation is that the larger the inner/middle diameters are, the smaller are the differences between the metallic/semiconducting shielding effects, which can be observed in Figure 3 for the range between 0.8 and 0.9 nm. A more detailed discussion about this C_e -metallicity dependence will be the focus of further investigations.

To locate, distinguish, and characterize **individual TWNTs** with various E_{laser} lines, gold grids were prepared on a silicon substrate (see Figure 4a). The 1 μm thick Au lines, which form different square sizes, allow a convenient location procedure, making possible the unambiguous identification of the location of each individual TWNT in the sample.¹⁸ Afterward we spin-coated a solution containing the TWNTs on the gold grid. First, using a motorized stage, we took Raman spectral maps from each square of the grid (one example can be seen in Figure 4b). Once we identified a potential area with an individual TWNT (for example see Figure 4b), high resolution RRS maps with a stage step-size of 100 nm in the x - and y -directions (the z -direction is normal to the Si substrate) were taken, as

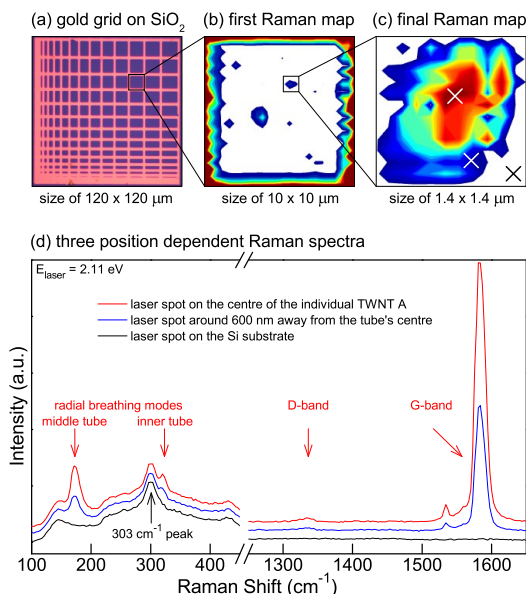


Figure 4. (a) The Au grid on a Si substrate is used to identify the location of the deposited TWNTs. Panels b and c show Raman maps of a specific area denoted by the Au markers. The color scale represents the intensity of the G-band, indicating the presence of carbon nanotubes. The three cross-symbols in panel c represent the locations from where the three Raman spectra were taken, which can be seen in panel d. The position dependent spectra in panel d show the RBMs, and the D-band and G-band of an individual TWNT (which is called TWNT A throughout the text).

shown in Figure 4c. In Figure 4b,c different colors represent the G-band intensities for the observed tubes. The average power used in these final Raman maps to measure the individual tubes was 7 mW with an acquisition time of 7 s. By doing this, we obtained in the Raman signal a clear identification of the tube positions and an explicit RBM observation. The spectral intensities and their dependency on the laser spot position are shown in Figure 4d. As shown in Figure 4d, in the low Raman frequency range (from 100 to 450 cm^{-1}) there are two RBM features, which correspond to the inner and middle tubes of an individual TWNT. Moving to higher spectral ranges (from 1250 to 1650 cm^{-1}), we have the D-band and G-band signals, which come from the same TWNT. In the following analysis we always took the Raman spectra from the point with the highest Raman signal which we identify with the best fit to the resonant window. It is important to comment that, due to signal filtering procedures, which are accomplished by a set of long-pass filters used to get rid of the elastic scattering contributions as well as stray light, the Raman spectra are all cut off at around 140 cm^{-1} . Therefore, any RBM information below this frequency is not accessible. For this reason, the outer tubes composing the TWNT structures were indirectly determined by means of their G-band and G'-band features. Additionally, AFM measurements were performed to give us further information about the tube density in the sample and about the height (which is

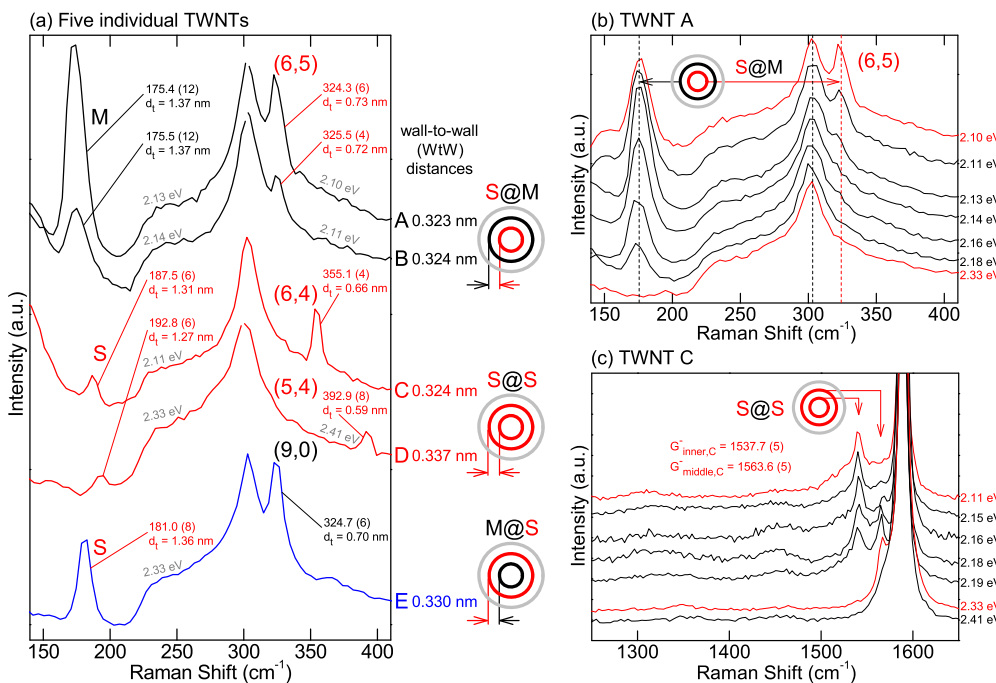


Figure 5. (a) The spectra show the RBMs of the inner and middle tubes of five individual TWNTs, marked with capital letters (A–E). Three flavors (S@M, S@S, and M@S) for the inner, individual DWNTs can be seen. We estimated the WtW distance which is according to eq 1 in the range from 0.323 to 0.337 nm. (b) The spectra represents the RBM resonance evolution of the TWNT A with a S@M DWNT flavor. The RBM of the metallic middle tube has its maximum intensity at 2.13 eV, in contrast to what occurs to the RBM of the semiconducting inner tube (6,5) between 2.10 and 2.13 eV. (c) Shown are the higher spectral ranges of the TWNT C taken by different E_{laser} . Here we see the absence of a significant D-band and the (decreasing) increasing of the G' occurrence for the semiconducting middle and inner tube.

associated with the outer tube diameter of the TWNT) from the substrate of the TWNTs that we measured.

The detailed RBM spectra for individual TWNT species are shown in Figure 5a. We found five distinct individual TWNTs (labeled with letters from A to E), with three different flavors (S@M, S@S, and M@S) for the inner, individual DWNTs. We plotted those spectra exhibiting the strongest RBM intensities, which we identify with the peak frequencies (note that spectra A, B, and D are split near the Si 303 cm⁻¹ peak). The two upper spectra (A and B) show inner, individual DWNTs with the S@M combination. Two DWNTs (C and D) are identified with the S@S configuration and one DWNT (E) consists of the M@S combination. All inner tubes are in the RBM frequency range from 324 to 393 cm⁻¹ and the middle tubes are between 175 and 193 cm⁻¹. Each RBM is labeled with its fitted ω_{RBM} and fwhm values, as well as its corresponding d_t , which was found according to eq 1, considering the above quoted values for C_e . The RBM observation makes clear, that by a smaller diameter size of the middle tube, the diameter of the encapsulated fullerenes are also getting smaller by keeping the WtW distance of all five DWNTs in the range from 0.323 to 0.337 nm. The figure also clarifies that the RBM-FWHMs of the middle tubes differ from metallic tubes with RBM-FWHMs of 12 cm⁻¹ to semiconducting tubes with RBM-FWHMs between 6–8 cm⁻¹. The (5,4) tube from TWNT D is likely one of the smallest tubes which can be produced by

encapsulating fullerenes, because the minimal diameter for the host tubes is believed to be at 1.17 nm.²⁷ In addition, we plotted these five inner individual DWNTs in Figure 2 as pairs of symbols on top of the Kataura plot. By including the ω_{RBM} values of the inner tubes of the five individual TWNTs in Figure 3 (represented as filled symbols), we directly determine intertube interaction effects because of the frequency shift of an individual tube in comparison to the bundled values. All the semiconducting inner tubes (A–D) are up-shifted in frequency for the individual TWNT which indicates more high-curvature intertube interaction effects. In contrast, the metallic inner tube (E) shows no significant shift even with a WtW distance of 0.330 nm to the middle tube.

AFM height profile measurements of the individual TWNTs (TWNT A is seen in Figure 1c) show that the diameters of the outer tubes are around 1.95 ± 0.10 nm. This is in the range where we would expect the outer diameters of our individual TWNTs to be if we assume a WtW distance between the middle and outer tubes of 0.330 nm. The RBM frequencies for these outer tubes are expected to be around 130 cm⁻¹. In comparison to other reported RRS studies including our ω_{RBM} vs d_t relation, the WtW distance of 11 individual (6,5)@M peapod-derived DWNTs²⁰ range from 0.284 to 0.316 nm, and the WtW distance of two individual (9,1)@M peapod-derived DWNTs¹⁹ is calculated to be 0.317 and 0.323 nm. The WtW distance in TWNT systems ranges from 0.323 to 0.337 nm, which is larger than the WtW distance of

individual DWNTs and is coming closer to the interlayer distance in bulk graphite,²⁸ which is found to be 0.335 nm.

As regards resonance profiles, an example of the E_{laser} -dependent resonant Raman spectra of the RBM intensities from the two inner tubes of the individual TWNT A is shown in Figure 5b. It is observed that the RBM of the metallic middle tube is resonant with all available E_{laser} lines provided by the rhodamine dye that was used, with the laser lines ranging from 2.10 to 2.18 eV, with an intensity maximum at 2.13 eV. On the other hand, we notice that the RBM of the semiconducting inner tube (6,5) starts to appear at 2.13 eV. In plotting the RBM resonant windows for all five individual, inner DWNTs, two experimental findings are observed: First, the resonant windows for semiconducting and metallic tubes are around 0.10–0.15 eV. Second, each tube's RBM intensity behaves independently of their respective concentric neighbor tube's RBM intensity. Because of this, we can exclude the proposed behavior of a mechanical coupling of the RBMs between the concentric tubes, which was thought to introduce the called breathing-like phonon modes.^{29,30} Figure 5c shows that the spectral intensity for the TWNT C changes with E_{laser} . The absence of the D-band in all the presented spectra of TWNT C and of all other individual TWNTs (another example is seen in Figure 4d) indicates the preparation of TWNTs with high structural perfection. Note that the G-band modes of the TWNT C in Figure 5c shows two sharp G[−] features coming from the inner $G_{\text{inner,C}} = 1537.7 \text{ cm}^{-1}$ and middle $G_{\text{middle,C}} = 1563.6 \text{ cm}^{-1}$ semiconducting tube. Both peaks have the same fwhm of 5 cm^{-1} fitted to the spectra taken with the highest G[−] intensity. These TO modes of SWNTs are diameter dependent as is well-known in the literature.^{31,32} It is clear to observe, that both G[−] peaks decrease and increase differently in intensity by changing the laser excitation energy. Thus, $G_{\text{inner,C}}$ disappears by switching from the rhodamine dye to the Nd:YAG laser; in contrast $G_{\text{middle,C}}$ disappears at the lowest excitation energy of the

rhodamine dye laser, respectively, at 2.11 eV. Moreover, we characterized the G[−] peaks for all other semiconducting inner tubes of the TWNT A, B, and D. Both values of $G_{\text{inner,A}} = 1536.6 \text{ cm}^{-1}$ (fwhm = 5 cm^{-1}) and $G_{\text{inner,B}} = 1537.1 \text{ cm}^{-1}$ (fwhm = 5 cm^{-1}) belong to a (6,5) tube with diameters of 0.73 and 0.72 nm. The results for the TWNTs (A and B) can be directly compared with the 11 individual peapod-derived DWNTs reported in ref 20 where some similarities can be found. For the inner high-curvature (5,4) tube of the TWNT D with a diameter of 0.59 nm, we found a TO mode at $G_{\text{inner,D}} = 1511.5 \text{ cm}^{-1}$ (fwhm = 7 cm^{-1}). All resonant windows of the semiconducting G[−] peaks are around 0.30 eV.

CONCLUSION

We presented the first detailed RRS characterization of bundled and individual TWNTs, confirmed the synthesis method, and determined the high-quality of the TWNTs produced by our synthesis method. Our analysis showed in detail, that the inner peapod-derived nanotubes in the DWNT and TWNT systems have similar properties, and in both cases these nanotubes are flavor-dependent isolated. Inner semiconducting tubes are more affected by their surroundings and by high-curvature intertube interactions in contrast to metallic tubes. These inner metallic tubes show a similar behavior to supergrown²⁵ SWNTs, and this isolation-property could be interesting for nanoscience applications. The measurement strategy in combination with the sensitive Raman setup that was utilized made it possible to locate, distinguish, and characterize five individual TWNTs with three different flavors (S@M, S@S, and M@S) for the individual, inner DWNTs. The well-distinct RBMs represent long phonon lifetimes and with the proposed ω_{RBM} vs d_t relations we calculated the WtW distances of the two inner tubes of individual TWNTs which yielded $0.330 \pm 0.007 \text{ nm}$. Finally, the RBM and G-band resonant windows of the individual TWNTs helped us to make further observations/statements about high-curvature intertube interactions in DWNT and TWNT systems.

MATERIALS AND METHODS

In the past, highly pure and crystalline DWNTs with small diameters were prepared by the judicious combination of the CCVD method and a two-step oxidative purification process.^{33–35} However, the inner tubes of the catalytically grown DWNTs, with diameters of 0.5–1.0 nm, are too small to encapsulate fullerenes. Thus, to prepare DWNTs with larger-diameters so that they could encapsulate fullerenes later, the DWNTs were thermally treated at 2400 °C in argon using a graphite furnace.¹¹ Such a high-temperature treatment allows us to prepare large-diameter DWNTs via the coalescence mechanism between adjacent tubes. Through this method, we found that the inner diameters of the thermally treated DWNTs were mainly in the range of 1.2–1.6 nm, which is reasonable for encapsulating the peapods. To remove the cap-structure of the DWNTs, an air-oxidation treatment was carried out in an air atmosphere, the oxidized DWNTs and fullerenes were sealed into a glass tube under vacuum, and finally the mixture was

annealed at 600 °C for 5 h. DWNTs encapsulating fullerenes were prepared after removing the residual fullerenes attached to the surface of the DWNTs by using a toluene solvent. The filling fraction of fullerenes within the DWNTs was estimated to be ~40% using high resolution transmission electron microscopy (HRTEM) observations.¹¹ To transform DWNT-peapods into TWNTs, a high-temperature thermal treatment was carried out for 30 min at temperatures of 2000 °C using a graphite furnace in argon. The purity of the TWNTs in comparison to the SWNTs and DWNTs was calculated to be 45% by considering the filling ratio as well as the conversion rate of the peapods, which is in reasonable agreement with the observations.

In all RRS experiments we used the following lasers: A Nd:YAG laser, an argon ion laser, two tunable dye lasers (DCM and rhodamine dye), and a Ti:sapphire laser. To collect the Raman spectra we used a thermoelectrically cooled Si charge coupled device (CCD) detector operating at -75°C . A 100 \times objective was used in a backscattering geometry for the data collection.

Conflict of Interest: The authors declare no competing financial interest.

Acknowledgment. We thank F. Villalpando-Paez, J. Kong, and W. Gaviria for stimulating discussions and experimental support. T.C.H. thanks the Prof. Dr.-Ing. Erich Müller Foundation for the financial support in the form of a MIT visiting-student scholarship. H.M. acknowledges support from the JSPS KAKENHI Grant Number 24710115. P.T.A. and M.S.D. acknowledge the NSF-DMR 10-04147 grant.

Note Added after ASAP Publication: This paper published ASAP on January 23, 2013 with an incorrect citation in the Results and Discussion section. The revised version was reposted on January 25, 2013.

REFERENCES AND NOTES

- Craciun, M. F.; Russo, S.; Yamamoto, M.; Oostinga, J. B.; Morpurgo, A. F.; Tarucha, S. Trilayer Graphene is a Semimetal with a Gate-Tunable Band Overlap. *Nat. Nanotechnol.* **2009**, *4*, 383–388.
- Lui, C. H.; Li, Z.; Mak, K. F.; Cappelluti, E.; Heinz, T. F. Observation of an Electrically Tunable Band Gap in Trilayer Graphene. *Nat. Phys.* **2011**, *7*, 944–947.
- Brown, L.; Hovden, R.; Huang, P.; Wojcik, M.; Muller, D. A.; Park, J. Twinning and Twisting of Tri- and Bilayer Graphene. *Nano Lett.* **2012**, *12*, 1609–1615.
- Shen, C.; Brozena, A. H.; Wang, Y. H. Double-Walled Carbon Nanotubes: Challenges and Opportunities. *Nanoscale* **2011**, *3*, 503–518.
- Jorio, A.; Saito, R.; Hafner, J. H.; Lieber, C. M.; Hunter, M.; McClure, T.; Dresselhaus, G.; Dresselhaus, M. S. Structural (*n,m*) Determination of Isolated Single-Wall Carbon Nanotubes by Resonant Raman Scattering. *Phys. Rev. Lett.* **2001**, *86*, 1118.
- Dresselhaus, M. S.; Dresselhaus, G.; Saito, R.; Jorio, A. Raman Spectroscopy of Carbon Nanotubes. *Phys. Rep.* **2005**, *409*, 47–99.
- Araujo, P. T.; Doorn, S. K.; Kilina, S.; Tretiak, S.; Einarsson, E.; Maruyama, S.; Chacham, H.; Pimenta, M. A.; Jorio, A. Third and Fourth Optical Transitions in Semiconducting Carbon Nanotubes. *Phys. Rev. Lett.* **2007**, *98*, 067401.
- Doorn, S. K.; Araujo, P. T.; Hata, K.; Jorio, A. Excitons and Exciton-Phonon Coupling in Metallic Single-Walled Carbon Nanotubes: Resonance Raman Spectroscopy. *Phys. Rev. B* **2008**, *78*, 165408.
- Xu, Z.; Li, H.; Fujisawa, K.; Kim, Y. A.; Endo, M.; Ding, F. Multiple Intra-tube Junctions in the Inner Tube of Peapod-Derived Double Walled Carbon Nanotubes: Theoretical Study and Experimental Evidence. *Nanoscale* **2012**, *4*, 130–136.
- Smith, B. W.; Monthoux, M.; Luzzi, D. E. Encapsulated C₆₀ in Carbon Nanotubes. *Nature* **1998**, *396*, 323–324.
- Muramatsu, H.; Shimamoto, D.; Hayashi, T.; Kim, Y. A.; Terrones, M.; Endo, M.; Dresselhaus, M. S. Bulk Synthesis of Narrow Diameter and Highly Crystalline Triple-Walled Carbon Nanotubes by Coalescing Fullerene Peapods. *Adv. Mater.* **2011**, *23*, 1761–1764.
- Hernandez, E.; Meunier, V.; Smith, B. W.; Rulari, R.; Terrones, H.; Buongiorno Nardelli, M.; Terrones, M.; Luzzi, D. E.; Charlier, J.-C. Fullerene Coalescence in Nanopeapods: A Path to Novel Tubular Carbon. *Nano Lett.* **2003**, *3*, 1037–1042.
- Kataura, H.; Kumazawa, Y.; Maniwa, Y.; Umezu, I.; Suzuki, S.; Ohtsuka, Y.; Achiba, Y. Optical Properties of Single-Wall Carbon Nanotubes. *Synth. Met.* **1999**, *103*, 2555–2558.
- Samsonidze, G. G.; Saito, R.; Kobayashi, N.; Gruneis, A.; Jiang, J.; Jorio, A.; Chou, S. G.; Dresselhaus, G.; Dresselhaus, M. S. Family Behavior of the Optical Transition Energies in Single-Wall Carbon Nanotubes of Smaller Diameters. *Appl. Phys. Lett.* **2004**, *85*, 5703–5705.
- Jorio, A.; Fantini, C.; Pimenta, M. A.; Capaz, R. B.; Samsonidze, G. G.; Dresselhaus, G.; Dresselhaus, M. S.; Jiang, J.; Kobayashi, N.; Gruneis, A.; et al. Resonance Raman Spectroscopy (*n,m*)-Dependent Effects in Small-Diameter Single-Wall Carbon Nanotubes. *Phys. Rev. B* **2005**, *71*, 075401.
- Araujo, P. T.; Maciel, I. O.; Pesce, P. B. C.; Pimenta, M. A.; Doorn, S. K.; Qian, H.; Hartschuh, A.; Steiner, M.; Grigorian, L.; Hata, K.; et al. Nature of the Constant Factor in the Relation between Radial Breathing Mode Frequency and Tube Diameter for Single-Wall Carbon Nanotubes. *Phys. Rev. B* **2008**, *77*, 241403 (R).
- Araujo, P. T.; Pesce, P. B. C.; Dresselhaus, M. S.; Sato, K.; Saito, R.; Jorio, A. Resonance Raman Spectroscopy of the Radial Breathing Modes in Carbon Nanotubes. *Phys. E* **2010**, *42*, 1251–1261.
- Villalpando-Paez, F.; Son, H.; Nezich, D.; Hsieh, Y. P.; Kong, J.; Kim, Y. A.; Shimamoto, D.; Muramatsu, H.; Hayashi, T.; Endo, M.; et al. Raman Spectroscopy Study of Isolated Double-Walled Carbon Nanotubes with Different Metallic and Semiconducting Configurations. *Nano Lett.* **2008**, *8*, 3879–3886.
- Villalpando-Paez, F.; Moura, L. G.; Fantini, C.; Muramatsu, H.; Hayashi, T.; Kim, Y. A.; Endo, M.; Terrones, M.; Pimenta, M. A.; Dresselhaus, M. S. Tunable Raman Spectroscopy Study of CVD and Peapod-Derived Bundled and Individual Double-Wall Carbon Nanotubes. *Phys. Rev. B* **2010**, *82*, 155416.
- Villalpando-Paez, F.; Muramatsu, H.; Kim, Y. A.; Farhat, H.; Endo, M.; Terrones, M.; Dresselhaus, M. S. Wall-to-Wall Stress Induced in (6,5) Semiconducting Nanotubes by Encapsulation in Metallic Outer Tubes of Different Diameters: A Resonance Raman Study of Individual C₆₀-Derived Double-Wall Carbon Nanotubes. *Nanoscale* **2010**, *2*, 406–411.
- Pfeiffer, R.; Simon, F.; Kuzmany, H.; Popov, V. N. Fine Structure of the Radial Breathing Mode of Double-Wall Carbon Nanotubes. *Phys. Rev. B* **2005**, *72*, 161404 (R).
- Pfeiffer, R.; Kramberger, C.; Simon, F.; Kuzmany, H.; Popov, V. N.; Kataura, H. Interaction between Concentric Tubes in DWCNTs. *Eur. Phys. J. B* **2004**, *42*, 345–350.
- Pfeiffer, R.; Simon, F.; Kuzmany, H.; Popov, V. N.; Zolyomi, V.; Kurti, J. Tube–Tube Interaction in Double-Wall Carbon Nanotubes. *Phys. Status Solidi B* **2006**, *243*, 3268–3272.
- Pfeiffer, R.; Holzweber, M.; Peterlik, H.; Kuzmany, H.; Liu, Z.; Suenaga, K.; Kataura, H. Dynamics of Carbon Nanotube Growth from Fullerenes. *Nano Lett.* **2007**, *7*, 2428–2434.
- Hata, K.; Futaba, D. N.; Mizuno, K.; Namai, T.; Yumura, M.; Iijima, S. Water-Assisted Highly Efficient Synthesis of Impurity-Free Single-Walled Carbon Nanotubes. *Science* **2004**, *306*, 1362–1364.
- Endo, M.; Kim, Y. A.; Hayashi, T.; Muramatsu, H.; Terrones, M.; Saito, R.; Villalpando-Paez, F.; Chou, S. G.; Dresselhaus, M. S. Nanotube Coalescence-Inducing Mode: A Novel Vibrational Mode in Carbon Systems. *Small* **2006**, *2*, 1031–1036.
- Melle-Franco, M.; Kuzmany, H.; Zerbetto, F. Mechanical Interactions in All-Carbon Peapods. *J. Phys. Chem. B* **2003**, *107*, 6986–6990.
- Bacon, R. Growth, Structure, and Properties of Graphite Whiskers. *J. Appl. Phys.* **1960**, *31*, 283–290.
- Popov, V. N.; Henrard, L. Breathinglike Phonon Modes of Multiwalled Carbon Nanotubes. *Phys. Rev. B* **2002**, *65*, 235415.
- Levshov, D.; Than, T. X.; Arenal, R.; Popov, V. N.; Parret, R.; Paillet, M.; Jourdain, V.; Zahab, A. A.; Michel, T.; Yazyuk, Yu. I.; et al. Experimental Evidence of a Mechanical Coupling between Layers in an Individual Double-Walled Carbon Nanotube. *Nano Lett.* **2011**, *11*, 4800–4804.
- Jorio, A.; Souza Filho, A. G.; Dresselhaus, G.; Dresselhaus, M. S.; Swan, A. K.; Ünlü, M. S.; Goldberg, B. B.; Pimenta, M. A.; Hafner, J. H.; Lieber, C. M.; et al. G-Band Resonant Raman Study of 62 Isolated Single-Wall Carbon Nanotubes. *Phys. Rev. B* **2002**, *65*, 155412.
- Pisanec, S.; Lazzeri, M.; Robertson, J.; Ferrari, A. C.; Mauri, F. Optical Phonons in Carbon Nanotubes: Kohn Anomalies, Peierls Distortions, and Dynamic Effects. *Phys. Rev. B* **2007**, *75*, 035427.
- Kim, Y. A.; Muramatsu, H.; Hayashi, T.; Endo, M.; Terrones, M.; Dresselhaus, M. S. Thermal Stability and Structural Changes of Double-Walled Carbon Nanotubes by Heat Treatment. *Chem. Phys. Lett.* **2004**, *398*, 87–92.
- Endo, M.; Muramatsu, H.; Hayashi, T.; Kim, Y. A.; Terrones, M.; Dresselhaus, M. S. Buckypaper from Coaxial Nanotubes. *Nature* **2005**, *433*, 476.
- Kim, Y. A.; Muramatsu, H.; Hayashi, T.; Endo, M.; Terrones, M.; Dresselhaus, M. S. Fabrication of High-Purity, Double-Walled Carbon Nanotube Buckypaper. *Chem. Vap. Deposition* **2006**, *12*, 327–330.